Evaluation of Aerodynamic Heating Uncertainties for Space Shuttle

R. V. MASEK*
McDonnell Douglas Astronautics Company-E, St. Louis, Mo.
AND
D. HENDER†
McDonnell Douglas Astronautics Company, Huntington Beach, Calif.
AND
J. A. FORNEY‡
NASA Marshall Space Flight Center, Huntsville, Ala.

The uncertainties in heating predictions derived from ground test data correlations have been used to define the corresponding uncertainties in TPS weight for the Space Shuttle. A completely reusable Shuttle system consisting of an aluminum heat sink booster and orbiter with reusable surface insulation for thermal protection was evaluated. The largest contribution to the uncertainty in TPS weight for the orbiter occurred on lower surface areas as a result of heating and boundary-layer transition uncertainties. Extension of this work to the current Shuttle system concept showed reduced weight uncertainty for the external tank compared to the reusable booster.

Nomenclature

$H(T)$, h, $H(0.9\text{TO})$, H	= heat-transfer coefficient
L	= model reference length (body axial length)
m	= meter
M	= Mach number
P	= pressure
$\dot{q}$	= heating rate
Re	= Reynolds number
Re_∞/L	= freestream unit Reynolds number
Re_θ	= momentum thickness Reynolds number
T	= temperature
V	= velocity
W	= TPS weight
X	= axial distance
α	= angle of attack
δ	= local flow deflection angle
ϕ	= peripheral angle
σ	= population standard deviation
t	= time
Δ	= increment in parameter prefixed

Subscripts

B	= booster alone
$B+O$	= booster mated with orbiter
$C.L.$	= lower surface centerline value
e	= edge condition
L	= local conditions
tr	= transition location
ϕ	= local peripheral value
∞	= freestream
s	= stagnation point
Ref	= reference value of h or $\dot{q}$ for a unit ($R = 1'$) sphere scaled to model size
w	= wall condition
i	= impingement region
u	= undisturbed

Presented as Paper 73-737 at the AIAA 8th Thermophysics Conference, Palm Springs, Calif., July 16–18, 1973; submitted August 20, 1973; revision received January 2, 1974.

Index categories: LV/M Aerodynamic Heating; Boundary Layers and Convective Heat Transfer—Laminar; Boundary Layers and Convective Heat Transfer—Turbulent.

* Project Thermodynamics Engineer. Member AIAA.
† Senior Engineer—Scientist. Member AIAA.
‡ Aerospace Engineer.

I. Introduction and Summary

QUANTITATIVE estimates have been made of the uncertainty in predicting aerodynamic heating rates for the Space Shuttle system, and the impact of these uncertainties on Thermal Protection System (TPS) weight. Widely differing temperature predictions for the Shuttle on the part of the several Phase A and Phase B contractors showed that such an effort was required, especially when the effect of vehicle weight increases on totally reusable system cost (e.g., $28,000 per lb for the orbiter based on MDC Phase B cost studies) is considered. This paper summarizes these effects for fully reusable Shuttle system (Phase B) and extends the results to the External Tank (Phase C/D) concept.

The estimates were based on statistical evaluations of the scatter of aerodynamic heating data obtained on Shuttle configuration about state-of-the-art (e.g., Phase B) heating prediction methods to define the uncertainty in these heating predictions. The uncertainties were then applied as heating rate increments to the nominal predicted heating rate to define the uncertainty in TPS weight. Separate evaluations were made for the reusable booster, reusable orbiter, and external tank, for trajectories which included boost through re-entry and touchdown.

Various prediction methods were investigated for application to local areas on the Shuttle configurations. The prediction methods were those recommended by the NASA Shuttle Aerodynamic Heating Panel, and alternate state-of-the-art methods. These included: 1) direct correlation of the wind-tunnel data for a specific configuration in terms of h/h_{ref}, i.e., normalization of heating data to Fay-Riddell theory; and 2) experimental determination of three-dimensional crossflow correction factors for candidate theories using data on a specified configuration.

For "best fits" of existing data to each method, multiplication factors corresponding to 1, 2, and 3 standard deviations of the data about the fit were determined and used to define the uncertainty in thermal protection system requirements.

Analyses were conducted for a completely reusable Shuttle system consisting of an aluminum heat sink fly-back booster and an orbiter which employed reusable surface insulation (RSI) for thermal protection. These analyses showed that the largest contribution to the uncertainty in TPS weight for the orbiter

occurred on lower surface areas as a result of the combined effect of heating and boundary-layer transition uncertainties. It was found that the major contribution to weight uncertainty for the booster was the uncertainty in wing heating because of the large area involved. Although the heat sink booster skin thickness was found to be very sensitive to heating uncertainties, this sensitivity did not translate directly into increased weight since a large portion of the booster is cryogenic tankage for which the skin thickness required for structure is greater than the thickness required to accommodate the heating uncertainties.

Analyses for the External Tank (ET) showed (as for the reusable booster) that the majority of the tank was sized by structural and/or ground hold requirements; therefore, the weight was unaffected by heating uncertainties. The intertank and retro motor fairing were found to require thermal protection for both nominal and off-nominal heating environments. The increased section weight resulting from these uncertainties was found to be small for cork ablative thermal protection.

II. The Aerothermodynamic Phenomena

Two Shuttle mission and configuration concepts were assumed: the fully reusable system developed in Phase B, and a reusable orbiter with expendable tanks and solid booster. Figure 1 shows in pictorial form the important mission phases for both concepts. The corresponding trajectory variables are defined in Ref. 1.

Reusable System Concept

During liftoff and boost, the orbiter is mated to the top of the booster. While in this configuration, prior to staging at approximately 2.135 km/sec (7000 fps), critical booster heating is encountered on the forward portion of the top of the booster fuselage because of bow shock intersections and channeled flow between the two vehicles. The flow is turbulent and (since radiation cooling of the surfaces is difficult as a result of shading by the other vehicle) temperatures may easily exceed material temperature limits.

During the separation maneuver, the aft upper fuselage encounters plume impingement heating from the orbiter engines. The booster is powered down and the attitude pitched to $\pi/3$ rad (60°) angle of attack, and booster re-entry is begun. Booster re-entry is accomplished at this fixed angle of attack throughout the hypersonic flight regime, during which lower surface heating is critical. As a result of the presence of wings and canards, heating because of shock impingement produces local hot spots on the side of the fuselage. Local heating increase may also occur on the wings on account of nose/wing shock interactions.

After vehicle separation, the orbiter engines deliver the vehicle to the planned orbit; the experiments or other orbital missions are accomplished; and the vehicle is prepared for re-entry. Except for abort or once-around missions, the boost phase heating to the orbiter is dissipated and the initial TPS temperatures are determined by the orbit, vehicle inclination, and thermal control provisions. Thus, the orbiter TPS is sized primarily by re-entry with the possible exception of certain regions on the upper surface which may become critical during boost.

External Tank System Concept

This system concept differs primarily in the degree of system reuse and allows a smaller, lighter weight orbiter. The configuration consists of a large external propellant tank mounted below the orbiter containing hydrogen and oxygen for the main engines of the orbiter. Additional propulsion is provided by two solid rocket motors (SRM) mounted on opposite sides of the external tank. The solid rocket motors are used to boost the vehicle to approximately 5000 fps and are dropped after staging. The main engines of the orbiter are then used to propel it into orbit. After orbit insertion the external tank is separated from the orbiter. Orbital missions and entry do not differ significantly from the fully reusable system. The low staging velocity for the SRM provides a moderate aerothermodynamic environment for these booster motors with no requirement for external heat protection. However, the external tank is carried into orbit and portions of the tank encounter significant heating on account of mated interference and plume radiation heating.

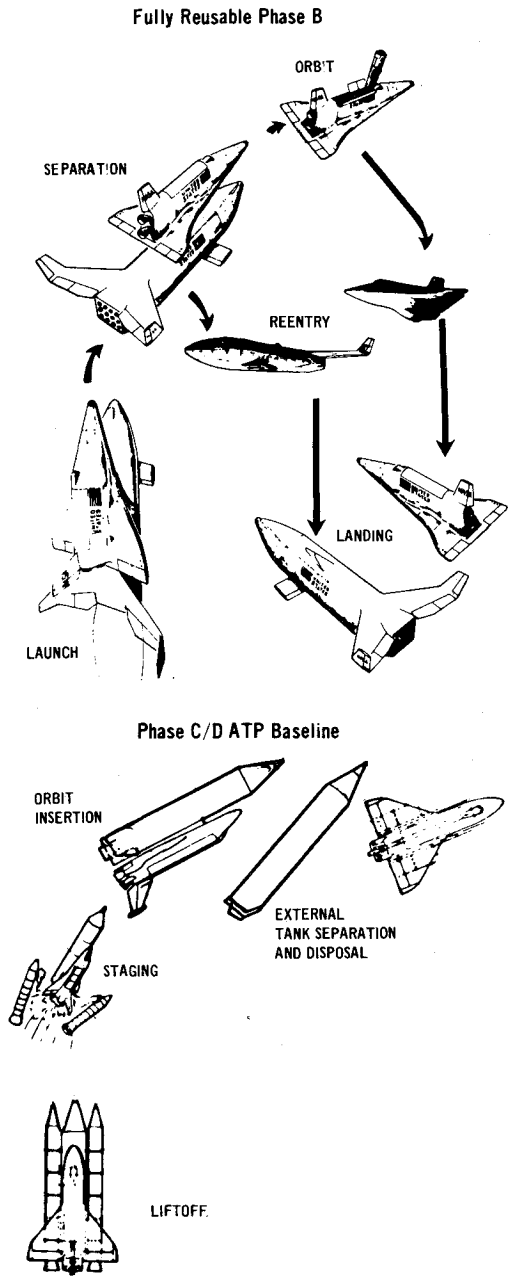

Fig. 1 Space shuttle system concepts.

III. Aerodynamic Heating Uncertainties

Aerodynamic heating correlations and uncertainties were derived from data obtained during Phase A and Phase B on the General Dynamic/Convair (GD/C) and McDonnell Douglas Corp. (MDC)/Martin booster, and Rockwell International (RI) and MDC orbiter configurations. The correlations were of two general types: curve fits to reported h/h_{ref} data and development of factors to relate the measurements to an appropriate theory. The theories with which the data were compared include the Eckert Reference Enthalpy, $\rho\mu$, and Beckwith and Gallagher, for turbulent flow conditions. Local flow properties were based on equivalent sharp cone flow except for the booster at 0° angle of attack, for which expansion from normal shock entropy was

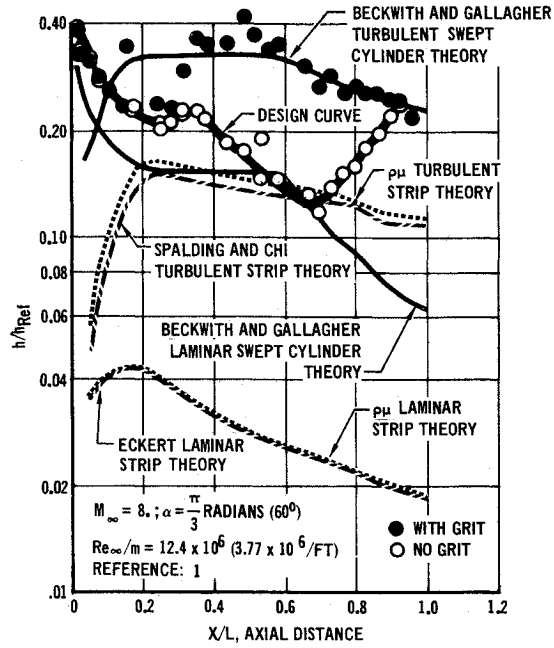

Fig. 2 GD/C B-15B-2 booster lower surface centerline heating distribution.

assumed. All theoretical calculations were performed with the MINIVER computer program developed by MDC and described in Ref. 2.

Lower Surfaces

Transitional and turbulent data taken at $\pi/3$ rad (60° angle of attack) on a GD/C booster configuration are compared with turbulent Spalding-Chi $\rho\mu$, and Beckwith and Gallagher swept cylinder results, and with a number of laminar theories, in Fig. 2. The Beckwith and Gallagher results show good agreement with the turbulent data, but the three-dimensional character of the flow prevented the laminar theories from matching the test results. Similar comparisons were made for other booster and orbiter configurations for the angle of attack range of 0 to $\pi/3$ rad (0°–60°). Resulting correlations for laminar and turbulent flow on an MDC orbiter configuration are shown in Fig. 3. For these data, the theoretical strip heating was modified to approximately correct for three-dimensional effects using the method of Ref. 3. The form of the data correlation and best fits were obtained from multiple regression analyses (MRA) of the parameter h_{DATA}/h_{THEORY} to identify its sensitivity to pertinent variables. A discussion of the MRA approach can be found in Ref. 4.

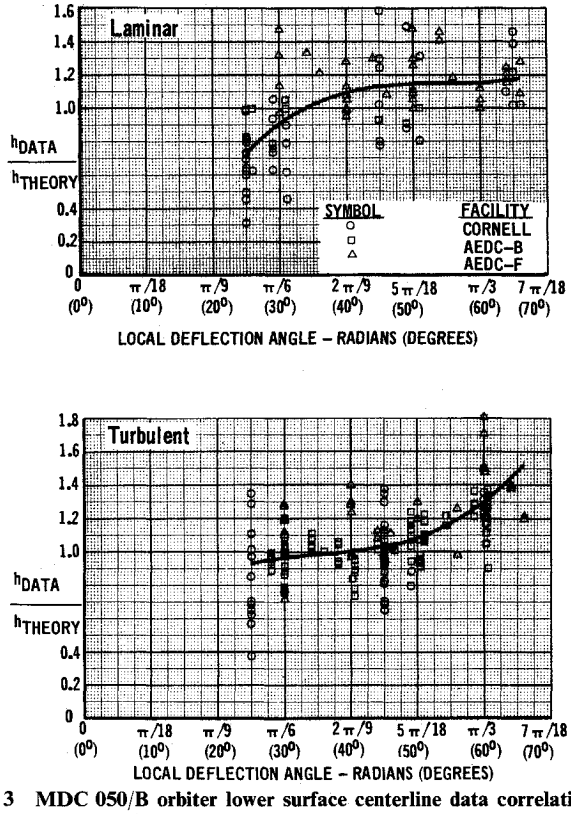

Fig. 3 MDC 050/B orbiter lower surface centerline data correlation.

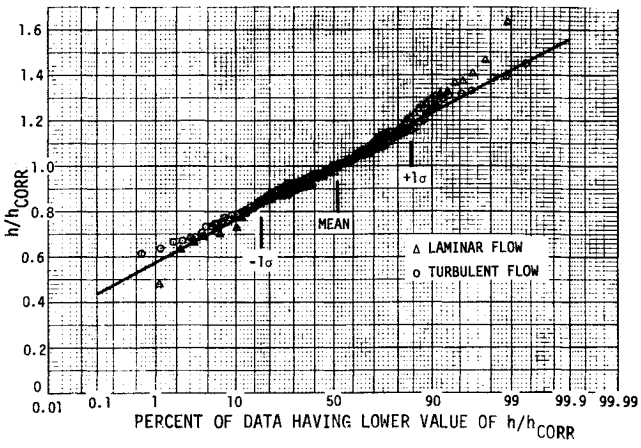

Fig. 4 MDC 050/B orbiter data scatter.

The standard deviation of the data which form the basis for defining the aerodynamic heating uncertainty was obtained graphically. This graphical technique provides a visual description of the data scatter distributions and a consistent method for deriving the standard deviation of the data set(s). Figure 4 contains the ratio of data to theory as a function of the percent of the data which lies below each value. Fits to the laminar and turbulent data of Fig. 3 are superimposed in the figure. It can be seen that the uncertainty in the laminar data is slightly greater than for the turbulent data. They are, however, sufficiently close that a single value could be used for each set. This value of the factor corresponding to one standard deviation is approximately 18%.

The slightly higher value for laminar flow had not been anticipated, since laminar theories are further advanced than those for turbulent flow (at least for stagnation point heating). Investigation of the reasons for this has indicated that the range of environment parameters was wider for the laminar than for the turbulent data and, in addition, that the laminar heating is more sensitive to three-dimensional flow effects, which are not perfectly modeled in the theory used in this analysis. A better explanation of this phenomenon requires a more complete data base or the development of more sophisticated flowfield and heating models for the complex shuttle configurations.

Peripheral heating data for both the straight and delta wing booster configurations were also correlated. The correlation took the form of $(h/h_{ref}) = f(\phi, \phi 2, \phi 3)$ with the angle ϕ measured from the lower surface centerline.

Interference Regions

The portions of the booster likely to be affected by interference are in the vicinity of the canard, the aft side body above the wing, and the upper surfaces during mated boost. During boost the vehicles are at zero angle of attack and the mated interference overpowers any canard effects.

Interference heating on the mated GD/C booster was evaluated using the data of Ref. 5. The test configuration was comprised of the RI 161B delta wing orbiter mounted piggyback to the GD/C B-15B-2 booster. The ratios of the local heat-transfer coefficients on the mated booster upper body to those on

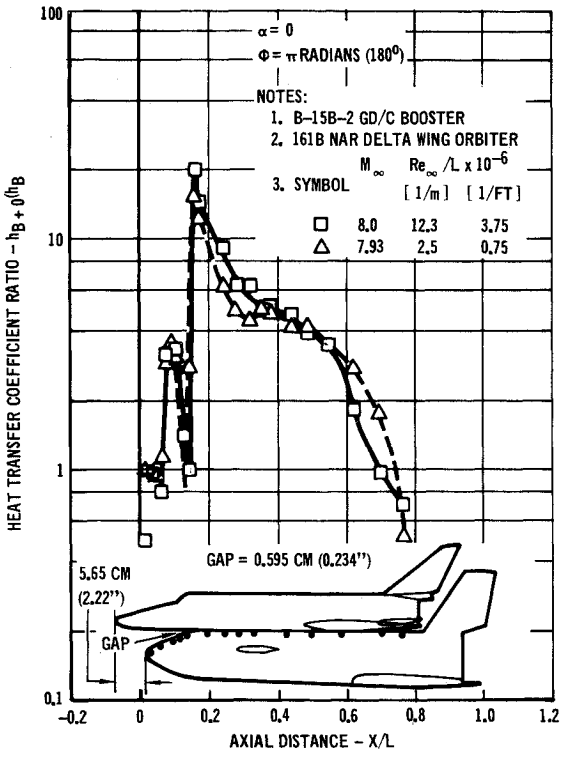

Fig. 5 Mated interference heating—GD/C booster.

the unmated booster were determined as a function of axial location. As may be seen in Fig. 5, heat-transfer coefficients on the mated booster in some locations are increased to values 20 times those on the booster alone.

A correlation of mated interference effects as a function of freestream Mach number, obtained from Ref. 6, is shown in Fig. 6. Superimposed on the data of the reference are the two peak values on the upper centerline of the B-15B-2 booster (Fig. 5). These data show very good agreement with the correlation and were therefore used to determine the nominal mated interference effects. The correlation assumes a Mach number dependence of the ratio of mated to unmated heating. Alternate correlations involving Reynolds number were also evaluated, but provided no better fit. The data scatter about this correlation is considerably larger than for windward areas unaffected by such flow interactions, since a correlating approach of much greater sophistication is necessary to model the aerothermodynamic phenomena.

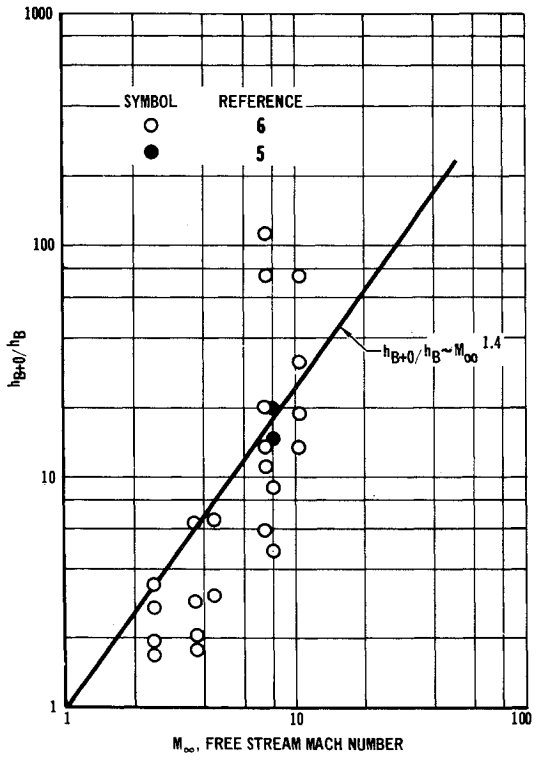

Fig. 6 Correlation of interference heat data.

Heating Uncertainties

Factors by which the nominal heating must be multiplied to account for the heating uncertainties, which were developed or described previously, are shown in Tables 1 and 2. These tables

Table 1 GD/C booster uncertainties

Vehicle location	Angle of attack	Flow	Off-nominal heating factor[a]	Sample size
Lower surface C.L.	0	lam	1.16	80
		turb	1.19	62
	$\pi/3(60°)$	lam	1.12	77
		turb	1.25	19
Windward peripheral	$\pi/6$ (30°)		1.28	78
Upper surface C.L.	0	lam	1.44[b]	22
		turb	1.44[b]	22
	$\pi/3$ (60°)	N.A.	1.27	40
Lower wing surface	0	lam	1.16	80
		turb	1.19	62
	$\pi/3$ (60°)	lam	1.12	77
		turb	1.25	19
Upper wing surface	0	lam	1.16	80
		turb	1.19	62
	$\pi/3$ (60°)	N.A.	$1\sigma = 1.83$ $2\sigma = 3.37$ $3\sigma = 6.21$	89
Above wing	0	N.A.	1.44[b]	22

[a] Ratio to nominal for 1σ (except as noted).
[b] Mated interference.

Table 2 MDAC delta wing orbiter uncertainties

Vehicle location	Angle of attack	Off-nominal heating factor[a]	Sample size
Lower surface centerline—All X/L	0 to $\pi/3$ (60°)	1.18	87
		1.18	166
span—$X/L = 0.5$	$\pi/6$ (30°)	1.31	27
$X/L = 0.75$		1.22	29
Upper surface centerline—forward of canopy	0.593 (34°)	1.25	45
aft of canopy	0.593 (34°)	1.45	45
Side body forward of wing	$\pi/6$ (30°)		
$X/L = 0.3$		1.35	24
$X/L = 0.45$		1.28	35
aft of wing $X/L = 0.68$		1.49	26
Upper wing	0.593 (34°)	$1\sigma = 2.04$ $2\sigma = 4.20$ $3\sigma = 8.75$	89

[a] For 1σ except as noted.

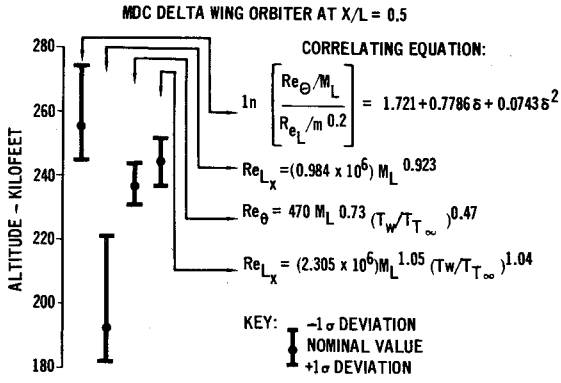

Fig. 7 Boundary-layer transition altitudes.

show that the largest uncertainty occurs in regions above the wing at high angles of attack. This is attributable to two factors: 1) the complex phenomena related to separated and reattaching flows which are poorly modeled in current correlations, and 2) the low heating levels in tests which are near the sensitivity level of the instrumentation.

Also, as expected, the regions where interference heating is present (upper surfaces of the booster at $\alpha = 0$) have high factors corresponding to one standard deviation of the data. The data scatter is slightly greater for the orbiter than for the booster. This is probably a result of the greater complexity of the flowfield (during re-entry).

Boundary-Layer Transition

In addition to heating factors applied to laminar and turbulent heating methods, an uncertainty exists in the state of the flow. This is best quantified as an uncertainty in the time of transition from laminar to turbulent flow, which can constitute a major contribution to the total uncertainty (since turbulent heating is a factor of two or more greater than the corresponding laminar values).

The transition data were treated similarly to the heat-transfer results. Best fits to a number of correlating approaches were made, and the standard deviation of the data about the best fit was determined graphically. Correlation parameters were developed by processing the wind-tunnel data with a multiple regression analysis computer program, assuming various combinations of parameters and forms of correlating equations.

Equations including Reynolds number, Mach number, flow deflection angle, and either the ratio of wall temperature to static temperature or the ratio of wall temperature to total temperature were found to yield low standard errors of estimate, i.e., a high degree of correlation. A minor improvement in the standard error of estimate was achieved by inclusion of unit Reynolds number, but the indicated dependency is slight.

Predicted transition altitudes and uncertainties corresponding to one standard deviation in the data about the fit are compared for a number of correlating approaches in Fig. 7. This chart shows the reduced uncertainty when wall temperature is included in the correlation. Care should be used in generalizing these results since it is well known that extrapolation of ground test transition data to flight is still questionable therefore, uncertainties based on both optimistic and conservative transition were evaluated and compared.

Scale to Flight

As previously discussed, the question of scaling uncertainties measured in ground test to the flight situation is not completely resolved. It is recognized that the ground test data contain sources of error which are not present in flight. Accuracy analyses by tunnel operators usually indicate that these error sources are small (although there is some indication that data taken by the Shuttle contractors using Stycast models may contain significant errors). If the instrumentation-related errors

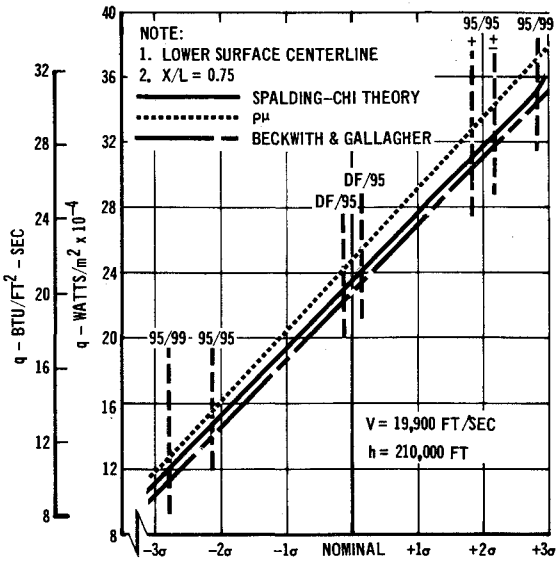

Fig. 8 Uncertainty in peak re-entry heating rate MDC 050/B orbiter.

are small compared with the total data scatter, it is likely that the major source of the scatter is the inability of theory to match the actual aerothermodynamic phenomena. This study was hampered by the limited quantity of data on similar configurations spanning large Mach number-Reynolds number ranges with wall cooling (e.g., T_w/T_{aw}) comparable with flight. As a result, conclusive proof that the wind-tunnel-derived uncertainties could be extrapolated to flight, could not be obtained. Therefore, various approaches to deriving uncertainty factors were compared for various confidence levels assuming one- or two-sided normal distributions of the data. The details of the statistics used in the evaluation can be obtained from Ref. 1. An example which corresponds to peak turbulent heating for the orbiter centerline is shown in Fig. 8.

Nominal and off-nominal heating corresponding to one, two, and three standard deviations of the data about each theory were made for the Spalding-Chi, Beckwith and Gallagher, and $\rho\mu$ turbulent theories. It is important to note that differences exist for the nominal case, since the theories extrapolate differently to the flight conditions. This occurs even though the standard deviations of the data about best fits for each theory were essentially the same at the flight angles of attack. Comparison of the data with theory could not, therefore, be used to select the theory which best modeled the test data.

Included on the curve are the heating rate excursions related to various statistical approaches and confidence levels. These include 95% confidence limits for the mean (indicated in the figure as DF) and confidence limits with tolerance for two-sided confidence levels for the data sample of 166 points. Because of the large sample size, the factor placed on the mean would be quite small and, if used as a design factor, would not even encompass the range of heating rates predicted in flight for nominal conditions by the three theories. In applying tolerance limits with confidence, it is recognized that the standard deviation is not precisely known, and, therefore, it is necessary to express for a given confidence level the percentage of the data which will fall in the interval. The intervals for 95% confidence, that 95% and 99% of the data will fall within, are also included in the figure. If the sample were infinite (the total population) the 95/95 location would be at 1.96σ. Also included on the figure are the values for 95/95 corresponding to one-sided confidence limits; that is, values corresponding to a 95% confidence level that the *peak* values will not be exceeded.

It is interesting to note that the use of two standard deviations to represent a 95% confidence level, the approach used previously in re-entry vehicle designs and also applied by Scottoline in Ref. 7, is midway between the 95/95 confidence limit with tolerance for one-sided and two-sided distributions.

Table 3 Combined structural and heat sink weight breakdown nominal MDAC-E transition criterion GD/C heat sink booster

Vehicle location	Nominal unit weight PSF	Nominal LB	$1\sigma^a$ LB	$3\sigma^a$ LB
Nose				
lower	7.48	18,803	23,773	34,166
upper	1.690	4,250	6,237	10,010
Body				
LOX tank—lower	2.81	5,893	5,893	7,383
LOX tank—upper	0.135	5,893	5,893	5,893
between tanks—lower	4.24	5,191	6,586	9,438
between tanks—upper	0.214	4,288	4,288	4,288
H_2 tank				
FWD lower	2.73	10,115	10,115	14,131
FWD upper	0.244	10,115	10,115	10,115
AFT lower	4.04	6,008	7,464	10,277
AFT upper	0.244	15,171	15,171	15,171
Aft H_2 tank				
lower	4.45	2,183	2,706	3,797
upper	0.680	1,002	1,489	2,550
Wing				
lower	6.91	45,693	56,566	80,074
upper	0.211	4,082	4,565	7,079
Total		138,687	160,861	214,372
Ratio to nominal		1.0	1.16	1.55

[a] σ based on uncertainty in heating rates.

Limited hypersonic data are available to compare scatter in flight with ground test results. Results for a slender axisymmetric configuration indicate that the three-dimensional effects are well modeled by the direct application of laminar ground test data and that the majority of the flight data are within two standard deviations of the ground test scatter. The turbulent flight data were found to be slightly lower than predicted by the ground test derived heating method (modified Spalding-Chi) but all measurements were lower than the prediction band corresponding to two standard deviations of the ground test results.

Because of limitations in the sample size and the large scatter present in the existing shuttle data, it does not appear justified to utilize highly sophisticated statistics to define confidence levels with tolerance since the difference in results from using the standard deviation, as a measure of confidence is small. However, it is recommended that future evaluations of aerodynamic heating uncertainties for application to Phase C/D use the more sophisticated approach, one-sided confidence limits with tolerance.

Booster TPS Requirements

The booster length was assumed to be 82 m (269 ft). The surface areas corresponding to each of the 14 regions for which the calculations were made are included in Fig. 9. It was assumed that the unit weight of the TPS was uniform for each region. Analyses for the booster assumed aluminum heat sink; that is, sufficient skin thickness was provided to limit the peak temperatures of the aluminum structure to 450°K (350°F). The LH_2 fuel and LOX tanks were assumed to be an integral part of the structure, and internal insulation was used to maintain preflight temperatures of the LH_2 tank above the LOX temperature 89°K (−300°F). In the nontank areas the liftoff temperature was assumed to be 300°K (80°F). The thermal analysis model assumed one-dimensional heat flow through the skin with an adiabatic back surface.

Table 3 contains the average aluminum skin weights for 14 locations on the booster for the nominal heat pulse and for heat pulses which are 1σ and 3σ higher than nominal These off-nominal values were obtained by applying appropriate heating multipliers from Table 1.

These results showed that the uncertainty in vehicle weight is approximately 55% for a confidence level of 99.7% (3σ). A review of the results shows that the major weight increment is on the wing lower surface. This occurs because of the large area involved. The average upper surface unit weights are considerably less than those on the lower surface, and thus have a smaller impact on the heat sink requirements.

Boundary-layer transition onset predictions used the MDAC-E-developed transition criterion which was recommended by the Shuttle Aerothermodynamic Working Group as an interim criterion during Phase B. Total vehicle weights were also computed to assess the effect of heating uncertainties for assumed completely laminar and completely turbulent flow. These showed that a weight reduction (from the nominal shown in Table 3) of 21,791 kg (48,041 lb) is possible, if the flow were laminar, and that a weight increase of 4270 kg (9413 lb) is possible, if the vehicle were designed for turbulent flow.

The effect of transition criterion on the TPS weight was also evaluated for uncertainties corresponding to the transition data scatter for $1\sigma, 2\sigma$, and 3σ. These results were combined statistically with the effect of uncertainty in heating rate. The combined weight uncertainty was obtained as the root sum square of the uncertainty resulting from heating rate prediction and boundary-layer transition data scatter. This is

$$\Delta W = [(\Delta W_q)^2 + (\Delta W_T)^2]^{1/2}$$

The nominal weight would need to be increased by 34,981 kg (77,118 lb) to assure a confidence level of approximately 99.7% (3σ) if the MDC transition criteria is used and 24,379 kg (53,746 lb) if a more optimistic transition criterion

$$Re_{L,x} = f(M_L^{0.923})$$

is utilized.

Orbiter TPS Requirements

Mullite RSI is attached through a foam layer to the aluminum structure. The use of mullite provides reusable capability to

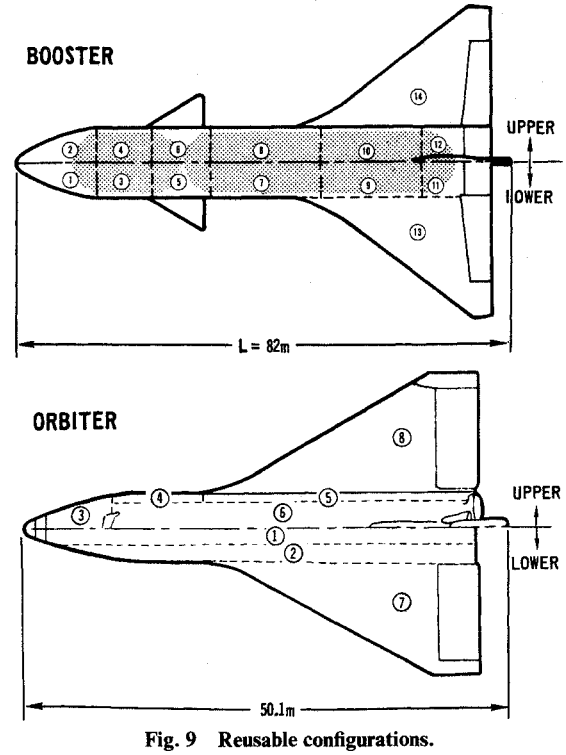

Fig. 9 Reusable configurations.

1350°K (2300°F) and overshoot capability to approximately 1860°K (2900°F). The foam layer is applied to isolate the RSI from the structural bending loads carried by the aluminum structure, thereby preventing potential damage to the RSI by structural buckling. The sizing of the RSI thickness and foam had two temperature constraints: an RSI-to-foam-bondline temperature limit of 590°K (600°F) and a peak aluminum structural temperature of 450°K (350°F). Because of handling and fabrication limits, the minimum thickness of RSI which can be applied is 0.635 cm (0.25 in.). The weights presented herein include the weight of RSI, its silicone waterproof coating, strain isolation foam, and adhesive required to bond the elements of the thermal protection system together. A structural aluminum thickness of 0.15 cm (0.06 in.) was assumed in these analyses.

The RSI was sized for re-entry only, since the small boost phase heat pulse will not produce critical bondline or structural temperatures and this heat will be dissipated during orbit for the majority of Shuttle orbiter missions. The possible exceptions to this case are abort or once-around missions. However, even for these remote situations, the boost phase is not likely to have a major effect on the sensitivities derived from this study for the re-entry heat pulse. The initial temperature of the TPS was assumed to be 311°K (100°F), a value consistent with normal vehicle attitude, orbital thermal control, and orbit inclination.

TPS requirements for the configuration shown in Fig. 9 were determined from correlations of the TPS unit weight as a function of integrated heat load. The TPS weight breakdown is summarized in Table 4. The weight breakdown includes weight for the eight sections into which the vehicle was divided. The nominal heat pulses and heat pulses corresponding to heating multipliers (derived from Table 2) for 1σ and 3σ uncertainties were used to define these TPS requirements. The MDC Phase B transition criterion was used in these analyses. The results show that the orbiter TPS weight is much less sensitive to the aerodynamic heating uncertainties than booster TPS weights, because the majority of the aerodynamic heating is reradiated to space. As the heating rate is increased, a greater fraction of the total heat is reradiated. Thus, the percent which is conducted to the structure is reduced. A 3σ design would require a 15% weight increase. The greatest weight penalty associated with the heating uncertainties is on the wing lower surfaces, primarily because of the large area involved. The locations having the largest uncertainties in heating are regions for which the nominal heating is quite low; it was found that only slight increases above minimum RSI thickness were required for the 3σ case in these areas.

Comparisons were made of results using the MDC and optimistic transition criteria, using the root sum square technique discussed previously. These showed that the 3σ design would be 2050 kg (4510 lb) heavier than the nominal using the MDC criterion and that the 3σ design would actually be 91 kg (200 lb) lighter than the nominal based on the MDC transition criterion, for a more optimistic transition assumption. This shows that the selection of the transition criterion to apply to the orbiter has a major influence on TPS weight, a situation which was not critical for the booster. The use of the optimistic criterion would result in a 3σ design approximately 13% lighter than would be predicted using the MDC criterion.

The abovementioned weight studies and tradeoffs were made under the implicit assumption that 1σ corresponds to a 68% confidence limit that the heating would not be exceeded in flight. As discussed previously, this use of the standard deviation to define confidence limits is not precise. Therefore, a more sophisticated approach which develops confidence limits with tolerance was also used to estimate the effects of heating uncertainties or orbiter TPS weight. To achieve a 95% confidence level that 95% of the data in flight will not exceed the design requirements (95/95), a 13% increase in TPS weight was required. For comparison, a corresponding 2σ design would require a 10% increase in weight. Thus, the use of more rigorous statistics results in slightly higher TPS weight uncertainties than derived from direct use of values of 1σ, 2σ, and 3σ.

Table 4 TPS weight breakdown nominal MDAC-E transition criterion MDAC DWO

Vehicle location	Nominal unit weight psf	Nominal lb	$1\sigma^a$ lb	$3\sigma^a$ lb
Nose	1.17	826	890	1,003
Lower surface	2.46	4,553	4,850	5,423
	2.36	4,368	4,665	5,683
Forward side	0.950	1,341	1,468	1,694
Aft side	0.911	2,511	2,511	2,839
Upper surface	0.911	3,198	3,198	3,247
Wing lower surface	2.51	10,063	10,704	12,388
Wing upper surface	0.911	3,387	3,387	3,387
Total studies		30,247	31,673	35,664
Remaining surfaces		6,895	6,895	6,895
Total		37,142	38,568	42,559
Ratio to nominal		1.0	1.04	1.15

[a] σ based on uncertainty in heating rates nominal transition criterion.

External Tank TPS Requirements

TPS requirements were determined for the tank of the Phase C/D ATP Baseline Shuttle launch configuration. The aerodynamic heating rates were computed in a manner similar to that used for the reusable booster.

Thermal protection system (TPS) unit weights were computed at the four locations on the external tank shown in Fig. 10 for nominal 1σ, 2σ, and 3σ thermal environments. These locations were selected since they are locations where aerodynamic heating uncertainties have the greatest impact on TPS section weights. They correspond to: 1) the stagnation point on the retro motor fairing; 2) the maximum Orbiter/tank interference heating location, which for the launch configuration analyzed, falls in the intertank region; 3) a point on the side of the tank which is subjected to interference heating from the solid rocket motor during its burn; and 4) a point on the bottom of the intertank structure, essentially free from any interference heating. These locations, rather than points on the propellant tanks, were

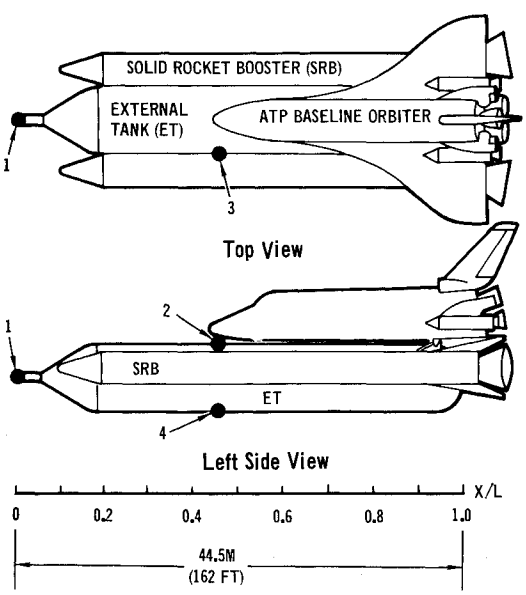

Fig. 10 Phase C/D ATP launch configuration.

Table 5 Effect of aerodynamic heating uncertainties on external tank TPS

Location	Environment	Ablator thickness (cm)	TPS section weight g/cm^{2a}	Increase in section wt. (%)
1	Nominal	0.855	0.759	...
	1σ	0.874	0.765	1.0
	2σ	0.902	0.780	3.0
	3σ	0.933	0.796	5.0
2	Nominal	0.297	1.642	...
	1σ	0.322	1.656	0.8
	2σ	0.335	1.662	1.2
	3σ	0.365	1.677	2.1

[a] Section weight includes seal or color coating and primer, adhesive for ablator (where required).

selected since they are not influenced by other heat sources (internal convection from the pressurant gas, ground hold heating to the hydrogen tank affecting propellant boiloff, and radiation to the aft surfaces of the hydrogen tank from the solid rocket motor exhaust plumes).

The design requirement used for these locations is a maximum aluminum substructure temperature of 149°C (300°F) until the tank is separated from the orbiter, in this case, at 966 sec from liftoff. When the heat sink capacity of the substructure would be exceeded without external protection, a TPS consisting of Armstrong 2755 Insulcork ablator was assumed.

The TPS weight requirements to accommodate these environments are shown in Table 5. It can be seen that cork is required to protect locations 1 and 2. The heat sink capacity of the average intertank skin is more than adequate to accommodate the 3σ deviations in aerodynamic heating for locations 3 and 4. It can also be seen that the TPS for locations 1 and 2 could be designed to accommodate the $+3\sigma$ aerodynamic heating levels with an increase in section weight of 5% or less. This small change in section weight results from the fact that the ablator weight increase, to absorb the additional heating, is small compared to the weight of the aluminum structure required to carry flight loads.

IV. Conclusions

This assessment of the effect of aerodynamic heating uncertainties on Space Shuttle TPS weights has identified the prediction methods for which improvement is most important. These include windward turbulent heating for the booster and orbiter. Mated interference heating was found to be less critical than initially suspected for the heat sink booster because the staging velocity was reduced from 10,000 to 7000 fps; and the apparent Mach number dependence of the interference heating effected a significant reduction in peak interference heating. Uncertainties in the heating to upper surface shielded regions at re-entry angles of attack were quite large. However, for the vehicle and TPS concepts studied in this program, the heat sink or RSI thickness in shielded regions was essentially sized by structural or manufacturing limitations. These uncertainties could, on the other hand, be critical for other configurations or TPS concepts.

The heat sink booster was found to be much more sensitive to aerodynamic heating uncertainties, and a high-confidence (3σ) design would be approximately 55% heavier (in skin and structure weight) than required if nominal heating is assumed. The equivalent penalty in TPS for the orbiter would be approximately 15%. The external tank in the Phase C/D ATP Shuttle concept is less affected by heating uncertainties than the orbiter because the structural requirements moderate the effect of aerodynamic heating uncertainties.

References

[1] Fehrman, A. L. and Masek, R. V., "Study of Uncertainties of Predicting Space Shuttle Thermal Environment," Final MDC Rept. E0639, June 30, 1972, McDonnell Douglas Corp., St. Louis, Mo.

[2] Hender, D., "A Miniature Version of the JA70 Aerodynamic Heating Computer Program, H800 (MINIVER)," MDC Rept. G0462, June 1970 (revised Jan. 1972), McDonnell Douglas Astronautics Co., Huntington Beach, Calif.

[3] Baranowski, L. C., "Influence of Crossflow on Windward Centerline Heating," MDC Rept. E0535, Dec. 23, 1971, McDonnell Douglas Corp., St. Louis, Mo.

[4] Ralston, A. and Wilf, H. S., *Mathematical Methods for Computers*, Wiley, New York, 1960, pp. 191–230.

[5] Warmbrod, J. D., Martindale, W. R., and Matthews, R. K., "Heat Transfer Rate Measurements on Convair Booster (B-15B-2) and Rockwell International Orbiter (151B) at Nominal Mach Number of 8," SADSAC Rept. DMS-DR-117, Nov. 1971, Chrysler Corp., New Orleans, La.

[6] Levine, B. M., "Interference Heating/CAL Test Program of MDC Delta Wing Orbiter/Booster," Data Analysis Report, McDonnell Douglas Corp., St. Louis, Mo. (to be published).

[7] Scottoline, C. A., "Determination of Aerothermodynamic Environment Uncertainties with Application to Space Shuttle Vehicles," Vol. II, TMX-2507, Feb. 1972, NASA.